Valence state and electronic structure of the misfit-layer compound $SmNbS_3$

1992 J. Phys.: Condens. Matter 4 7815

(http://iopscience.iop.org/0953-8984/4/38/012)

J. Phys.: Condens. Matter 4 (1992) 7815–7828. Printed in the UK

Valence state and electronic structure of the misfit-layer compound $SmNbS_3$

Youichi Ohno

Department of Physics, Faculty of General Education, Utsunomiya University, Mine-machi 350, 321 Utsunomiya, Tochigi, Japan

Received 23 March 1992, in final form 1 June 1992

Abstract. X-ray photoemission, x-ray absorption and reflection electron-energy-loss spectra of $SmNbS_3$ have been measured for the first time. The results give no clear evidence for valence fluctuation or the occurrence of mixed-valence states for Sm atoms. The Sm 4d and 3d x-ray photoemission spectra suggest that Sm exists mainly as a trivalent ion like the pressure-induced metallic phase of SmS, in agreement with a recent lattice parameter measurement. We have estimated that the number of Sm^{2+} ions is less than a few per cent of the number of Sm^{3+} ions, if they exist. Charge transfer from SmS layers to the incompletely filled Nb d_{z^2} band of NbS_2 layers has an important effect on the valence state of Sm and the disappearance of a shoulder near the Nb L_2 x-ray absorption edge. The Sm $N_{4,5}$ inner-shell-electron-energy-loss spectrum exhibits non-optical transitions below the threshold, as has already been observed for the elemental metal Sm. The valence and conduction bands are also discussed.

1. Introduction

$SmNbS_3$ belongs to the family of the misfit-layer compounds MTS_3 (M ≡ Sn, Pb, Bi, rare-earth metals; T ≡ Ti, V, Cr, Nb, Ta) which are built up of alternately stacked MS and TS_2 layers. The crystal structure has recently been determined precisely by Wiegers *et al* (1989, 1990) and Meerschaut *et al* (1991). The atomic arrangement within an MS layer is similar to that of a double layer in TII which resembles closely a rocksalt-like lattice sliced with two parallel planes perpendicular to a ⟨001⟩ direction and having an interplanar distance of half the lattice constant. In a real crystal, M atoms protrude slightly outside the planes; S atoms, on the other hand, sink into the planes. The atomic arrangement within a TS_2 layer is identical with that of a slab in a layered TS_2 compound and each T atom is surrounded octahedrally or trigonal-prismatically by six S atoms. Consequently the MS and TS_2 layers have different geometries. They are not represented by a single unit cell but are characterized by two centred orthorhombic unit cells mismatched along the a axis. The unit-cell parameters for $SmNbS_3$ are $a_1 = 5.570$ Å, $b_1 = 5.714$ Å and $c_1 = 22.514$ Å for the SmS part and $a_2 = 3.314$ Å, $b_2 = 5.714$ Å and $c_2 = 22.511$ Å for the NbS_2 part. The crystal structure is shown schematically in figure 1. The exact chemical composition is given by $(SmS)_{1.19}NbS_2$ where the value of 1.19 is deduced from the ratio $2(a_2/a_1)$.

To date, there have been few studies on the physical properties of $SmNbS_3$. Recently, Meerschaut *et al* (1991) measured the electrical resistivity as well as the

0953-8984/92/387815+14$04.50

magnetic susceptibility as functions of temperature, which showed superconductivity below 2.4 K. This critical temperature is smaller by 3.6 K than that of NbS_2. Our previous x-ray photoemission spectroscopy (XPS), x-ray absorption spectroscopy (XAS) and reflection electron-energy-loss spectroscopy (REELS) studies of $PbTiS_3$, $PbNbS_3$ and $SnNbS_3$ (Ohno 1991a, b) have shown that the electronic structures are well understood in terms of the energy band structure of each component compound, although charge transfer occurs from the MS to the TS_2 layers and a weak interlayer interaction exists, depending on the combination of two alternately stacked layers.

Two decades ago a semiconductor–metal phase transition was discovered in bulk SmS. The transition occurs by applying a high pressure of about 6.5 kbar to the crystal (Jayaraman *et al* 1970), by substituting trivalent anions such as P and As for some of the S atoms (Krill *et al* 1980) or by substituting cations of a smaller size than Sm^{2+}, e.g. Y, Gd and Th, for some of the Sm atoms (Jayaraman *et al* 1973, Campagna *et al* 1974). Many studies have been done to clarify understanding of the phenomenon. They have confirmed that the transition is caused by the electronic transition from a localized 4f level to a 5d conduction band or by the change in valence states of the Sm atoms. In pure semiconducting SmS, valence mixing is very small, less than about 3%, and Sm exists dominantly as a divalent ion, while in the metal phase these ions are in an interconfiguration fluctuation state and pronounced valence mixing occurs. A recent lattice parameter measurement for $SmNbS_3$ (Meerschaut *et al* 1991) has shown that the average Sm–S distance is comparable with that in the metal phase rather than that in the semiconducting phase. On the other hand, there are some experimental results which show a difference between chemically induced and pressure-induced metallic SmS. For example, $Sm_{1-x}Y_xS$ undergoes a metal–semiconductor phase transition at low temperatures in contrast with pressure-induced metallic SmS. Thus we are very interested in the valence state of Sm and the electronic structure of $SmNbS_3$.

This paper presents the XPS, XAS and REELS experimental studies of $SmNbS_3$. In XPS experiments the Sm 4d and 3d core spectra and the valence band spectrum have been measured to obtain information on the valence state of a Sm atom and occupied states near the Fermi level. In XAS experiments the Nb L_2 absorption spectrum which overlaps S K absorption in the high-energy region has been measured to give information on empty states near the Fermi level. In REELS experiments the Sm $N_{4,5}$ inner-shell-electron-energy-loss spectroscopy (ISEELS) spectrum and the valence-electron-excited REELS spectrum have been measured.

2. Experiments

Single crystals of $SmNbS_3$ were grown by the chemical vapour transport reaction in a silica ampoule of inner diameter 15 mm and of length about 300 mm which was evaculated and then sealed. The quantities of starting materials were determined, assuming the following reaction:

$$\tfrac{1}{2}Sm_2S_3 + (1-x)Nb + xNbCl_5 + \tfrac{3}{2}S \longrightarrow SmNbS_3 + \tfrac{5}{2}xCl_2$$

where $x = 0.05$. The resulting Cl_2 on the right-hand side was employed as a transport agent. The starting materials on the left-hand side were placed in a high-temperature zone of a three-zone electric furnace. In the first step they were heated at 900 °C for

a week to guarantee a homogeneous reaction. Single-crystal growth was performed in a temperature gradient of 960–860 °C. After a month, large thin crystals of diameter about 7 mm were grown together with powder in the high-temperature zone and leaf-like crystals of length about 20 mm were grown in the intermediate-temperature zone.

Structural and chemical analyses were done by means of the x-ray powder diffraction and the XPS techniques. The diffraction pattern of $SmNbS_3$ is similar to those of $PbNbS_3$ and $BiNbS_3$. Since in our pattern the $(0\,0\,l)$ lines predominate over the other lines, a detailed comparison with the diffraction data of Meerschaut *et al* (1991) cannot be made. Our estimated c-parameter is 22.44 Å, which is slightly smaller than their value (22.51 Å). Atomically clean and smooth surfaces for XPS and REELS measurements were prepared by cleaving with adhesive tape in the atmosphere just before the measurements. Auger electron spectroscopy (AES) spectra as well as core XPS spectra displayed small carbon and oxygen contaminant peaks, but argon ion sputtering and a subsequent annealing technique, which are customarily used to clean the surface, were not employed because they caused surface disorder and a non-stoichiometric surface chemical composition. We shall discuss the surface effects arising from oxygen adsorption and atomic rearrangement and estimate the contribution to the XPS spectra from measurements at different sampling depths.

The XPS spectra were measured with unmonochromatized Mg and Al Kα radiation, the excitation energies being 1253.6 eV and 1486.6 eV, respectively. A commercially available x-ray generator equipped with Mg and Al dual anodes was used as an x-ray source. The operating conditions were 15 kV and 20 mA. The energies of the ejected photoelectrons were anlaysed with a double-pass cylindrical mirror analyser (CMA) (Perkin–Elmer Instruments, model 15-255G). The binding energies were measured with respect to the Fermi level of a spectrometer, using the Cu $2p_{3/2}$ (932.4 eV) and C 1s (284.6 eV) lines as references. The vacuum system and the data acquisition and processing system were the same as those used in the REELS experiment. The Sm $N_{4,5}$ ISEELS spectrum and the valence-electron-excited REELS spectra were measured with a normal-incidence electron gun coaxial to the CMA. They were represented as an energy distribution curve or in the second-derivative form. Our REELS apparatus and data acquisition and processing system have been described in a previous paper (Ohno 1987).

The Nb L_2 and S K XAS spectra were measured with a vacuum soft-x-ray spectrometer of Johan type with a Rowland circle of radius 30 cm. The sample was prepared in the form of a thin film by rubbing fine powder onto a sheet of thin paper. The dispersing crystal was quartz with a $(10\bar{1}1)$ plane. The operating conditions of an x-ray tube were 4.0 kV and 24 mA. The x-ray detector was a gas-flow proportional counter with a 90 vol.% argon–10 vol.% methane gaseous mixture as the flow gas. A more detailed description of our apparatus and data acquisition and processing system has been given in a previous paper (Ohno *et al* 1983).

3. Results and discussion

XPS is a fast technique with a characteristic probing time of about 10^{-16} s. Thus it is a powerful means for investigating valence fluctuation in a mixed-valence system. In practice, Sm 4d and valence band XPS spectra give clear evidence for valence fluctuation in SmB_6 (Chazalviel *et al* 1976). Their spectra show structures arising from

divalent and trivalent Sm simultaneously in spite of equivalent chemical circumstances. Figure 2 shows the Sm 3d XPS spectrum of $SmNbS_3$ which has been measured with Al Kα radiation. The $3d_{5/2}$ and $3d_{3/2}$ structures are well separated by a large spin–orbit splitting of about 26 eV, but multiplet structures are not well resolved unlike the 4d spectrum because of a small d–f exchange interaction. The main peak, which is located at 1084.0 eV and 1110.5 eV for the $3d_{5/2}$ and $3d_{3/2}$ parts, respectively, is ascribed to the dominant Sm^{3+} $4d^9 4f^5$ final state. We also observe satellite peaks on the high- and low-energy sides. Since Al K$\alpha_{3,4}$ satellites are located at 9.8 and 16.8 eV below the main peak (Wagner *et al* 1979), the low-energy satellite may be attributed to the structures. However, the main peak for the Sm^{2+} $4d^9 4f^6$ final-state configuration is also located at the same energy, as confirmed for Sm metal and other mixed-valence compounds. If the low-energy satellite is regarded as due to Sm^{2+}-induced structures, $SmNbS_3$ is a mixed-valence compound although the mixing is very small. The overall features including energy positions are, however, quite similar to those of Sm_2O_3 where Sm exists as a trivalent ion. In table 1 we compare the energies of the main features of $SmNbS_3$, Sm_2O_3 and Sm metal. It is found that there is good agreement between $SmNbS_3$ and Sm_2O_3. We may suggest from the ratio of the area of the $3d_{5/2}$ main peak to the area of the low-energy satellite that Sm in $SmNbS_3$ exists dominantly as a trivalent ion, and the number of divalent ions is less than a few per cent of the number of trivalent ions, if they exist. A detailed discussion on the 3d XPS spectra of rare-earth metals and compounds has recently been given by Kotani (1987) and Jo and Kotani (1988), based on the impurity Anderson model incorporated with a core-hole potential.

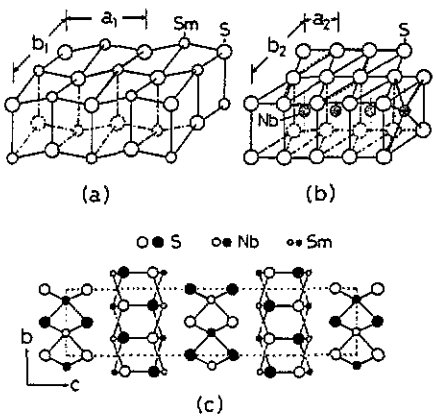

Figure 1. Crystal structure of $SmNbS_3$: (*a*) SmS layer; (*b*) NbS_2 layer, where Nb atoms are surrounded trigonal-prismatically by six S atoms; (*c*) unit cell of $SmNbS_3$ projected along the [100] axis, where the open and full circles denote atoms located at $x = 0$ and $x = \frac{1}{2}$, respectively.

Figure 3 shows the Sm 4d and S 2p XPS spectra which have been measured with Mg Kα radiation. Mg K$\alpha_{3,4}$ satellites are known to be located at 8.4 eV and 10.2 eV below the main peak. In our measurements, they are observed as a broad peak centred at 9.0 eV below the main peak. The 4d spectrum exhibits no well separated spin–orbit doublets and has more complicated features than the 3d spectrum has. The difference arises because the exchange interaction between 4d and 4f electrons

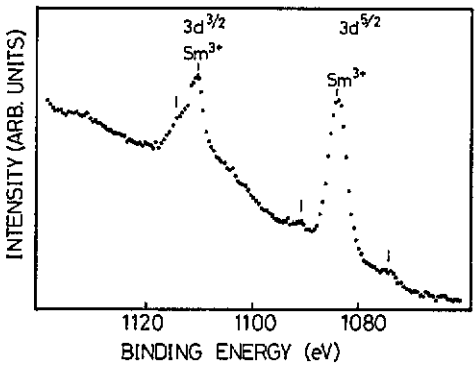

Figure 2. Sm 3d XPS spectrum of $SmNbS_3$ measured with Al Kα radiation.

Table 1. Energies of the main features of the Sm 3d XPS spectra of $SmNbS_3$, Sm_2O_3 and Sm metal.

Energy (eV)		
$SmNbS_3$	Sm_2O_3 [a]	Sm [a]
		1073.2
1074.0	1073.6	1075.4
1084.0	1083.4	1081.0
		1082.2
1091.0	1090.8	1088.0
1110.5	1110.8	1108.0
1114.0	1113.4	1111.0

[a] Dufour *et al* (1976).

is stronger than the spin–orbit interaction of about 2 eV. Thus the structures are interpreted in terms of the multiplet structures of the $4d^9 4f^5$ final state to the first approximation. Such an interpretation has been applied by Kowalczyk *et al* (1974) to explain the 4d XPS spectrum of Sm metal as well as the other rare-earth metals and has obtained great success. The Sm 4d spectrum of $SmNbS_3$ resembles that of Sm metal although the main features shift to higher energies by 2.2 eV with respect to those of Sm metal owing to the chemical shift of the 4d core electron. Even if a small structure near the threshold is not the Mg $K\alpha_{3,4}$ satellite of the Sm^{3+}-induced 4d structures but is the main peak of Sm^{2+}, valence mixing is very small. The probability of existence of Sm^{2+} ions is less than a few per cent. Here it is important to note that oxidization of the surface enhances Sm^{3+}, probably as the result of the formation of Sm_2O_3, while argon ion sputtering of the surface reduces Sm^{3+} and enhances Sm^{2+}, probably owing to structural disorder, which causes increased separation between Sm atoms. In the same manner we may also expect that a surface mixed-valence phase occurs as the result of atomic rearrangement or lattice relaxation near the surface, which causes an increase or decrease in the Sm–S and Sm–Sm distances. As described earlier, the surfaces of our XPS samples were contaminated by a small amount of oxygen, but they were not cleaned for the reason described above. Thus we may have overestimated the quantity of Sm^{3+}. Since the kinetic energy of excited 3d photoelectrons was about 400 eV, giving a small mean free path of several ångströms

while the kinetic energy of excited 4d photoelectrons was about 1200 eV, giving a larger mean free path of about 15 Å, then the 4d spectrum is less sensitive to the surface than is the 3d spectrum. Nevertheless both spectra lead to the same result for the quantities of Sm^{2+} and Sm^{3+} ions, suggesting that adsorbed oxygen and atomic arrangement near the surface have only unimportant effects on the valence state of Sm. This is because, since the compound is built up of alternately stacked SmS and NbS_2 layers which only weakly interact with each other, the cleaved surfaces are very stable chemically and structurally. Thus we may conclude that Sm in $SmNbS_3$ exists mainly as a trivalent ion as in Sm_2O_3, in agreement with the recent result obtained from the lattice parameter measurement (Meerschaut *et al* 1991). The S 2p spectrum reveals only a broad peak but has no obvious spin–orbit split peaks owing to different chemical circumstances within the SmS and NbS_2 layers.

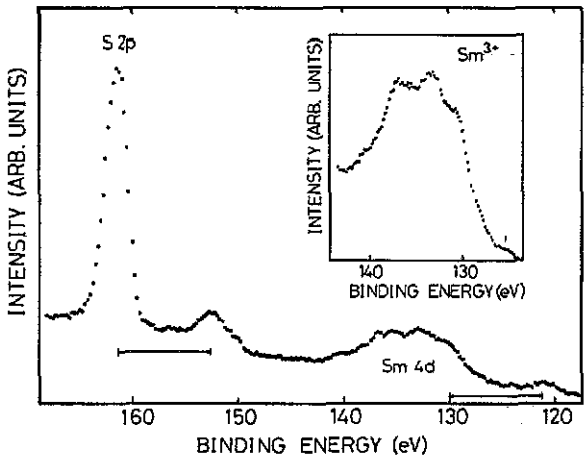

Figure 3. Sm 4d XPS spectrum of $SmNbS_3$ measured with Mg Kα radiation which involves the S 2p spectrum in the high-energy region. The inset is the Sm 4d spectrum at a high signal-to-noise ratio.

Figure 4 shows the valence band XPS spectrum involving the Nb 4p and Sm 5p core regions, and figure 5 shows a comparison between the valence band spectra of $SmNbS_3$ and of $NbSe_2$ (Wertheim *et al* 1973) and Sm^{3+} in Sm metal (Baer and Busch 1974). It is well known that the energy band structure of NbS_2 is quite similar to that of $NbSe_2$ and the Fermi level is located within a half-filled d_{z^2} band. For $SmNbS_3$ the valence band spectrum is divided into two parts. One is the upper valence band which consists of the Nb d_{z^2} and the S 3p bands of the NbS_2 layers and the well localized Sm 4f levels and the delocalized S 3p bands of the SmS layers. The other is the lower valence band which consists of the S 3s bands. As can be seen from figure 5, the main structures are explained in terms of the energy band structures of component compounds, taking into account that Sm exists as a trivalent ion. They are summarized in table 2. The top of the valence band consists of the Nb d_{z^2} band. The structures, d, e, f and g are the multiplet structures for the $4f^4$ final-state configuration of Sm^{3+}, superimposed by the S 3p bands of the NbS_2 and SmS layers. The combination experiment of XPS and ultraviolet photoemission spectroscopy (UPS) (Krill *et al* 1980) has shown that the S 3p bands of SmS are located at around 5 eV below the Fermi level. Because the energy resolution of our XPS spectrum is worse than the resolutions of the other spectra, we can give no clear evidence for charge

transfer from SmS layers to the Nb d_{z^2} band. Hence we have attempted to measure the Nb L_2 XAS spectrum which gives us information on the empty states near the Fermi level.

Table 2. Energies of the main features of the valence band XPS spectrum of $SmNbS_3$ (figure 5). The origin of the horizontal axis is the Fermi level.

Notation In figure 5	Energy (eV)	Assignment
a	1.0	Occupied states of the Nb d_{z^2} band
b	3.6	S 3p bands of an NbS_2 layer
c	4.8	S 3p bands of SmS and NbS_2 layers
d	5.5	Sm^{3+} $4f^4$ (^5I) multiplet superimposed by S 3p bands
e	7.0	Sm^{3+} $4f^4$ (^5F) multiplet superimposed by S 3p bands
f	7.8	Sm^{3+} $4f^4$ (^5G) multiplet superimposed by S 3p bands
g	9.6	Sm^{3+} $4f^4$ (^5D) multiplet superimposed by S 3p bands
h	13.0	S 3s bands of SmS and NbS_2 layers

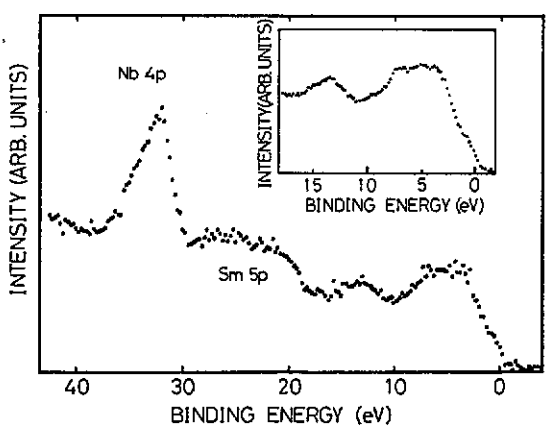

Figure 4. Valence band XPS spectrum of $SmNbS_3$ measured with Mg Kα radiation, which involves the Sm 5p and Nb 4p spectra in the high-energy region. The inset is the valence band spectrum at a high signal-to-noise ratio.

Figure 6 shows the near-edge structures of Nb L_2 and S K x-ray absorption for $SmNbS_3$, which are compared with those for NbS_2. The main-peak separation of Nb L_2 and S K absorption is 5.8 eV, in agreement with the energy difference between the absorption edges compiled by Bearden (1967). The previous XAS study of NbS_2 (Ohno *et al* 1983) confirmed a shoulder near the Nb L_2 and L_3 and the S K thresholds which originates from the empty states of the incompletely filled Nb d_{z^2} band. This shoulder reduces upon intercalation of Sn and Cu atoms because they are filled with transferred electrons from the inserted atoms (Ohno *et al* 1984). For $SmNbS_3$ the Nb L_2 absorption rises very smoothly. We cannot observe any structures near the threshold, and the difference spectrum which is obtained by subtracting the spectrum of NbS_2 from that of $SmNbS_3$ (the lowest spectrum in figure 5) shows a dip near the Nb L_2 and S K edges. A similar result has been obtained for $PbNbS_3$ and $SnNbS_3$ in which charge transfer occurs from the PbS or SnS layers to the NbS_2 layers (Ohno

1991b). Therefore it is considered that the shoulder disappears because the empty states of the Nb d_{z^2} band are filled with electrons transferred from the SmS layers. Summarizing the above facts, we may suggest that, for $SmNbS_3$, charge transfer occurs from the SmS to NbS_2 layers, resulting in a shift of the Fermi level within an NbS_2 layer and a change in the valence state of Sm within an SmS layer. The main peak of S K absorption is assigned to the remaining empty d bands hybridized with S 3p orbitals while the shoulder on the high-energy side is ascribed to the high density of empty states within an SmS layer. The latter assignment may be supported by the bremsstrahlung isochromat spectroscopy studies of Sm metal (Lang *et al* 1981) and heavily oxidized SmS (Oh and Allen 1984) which reveal the most prominent peak at around 4 eV above the threshold.

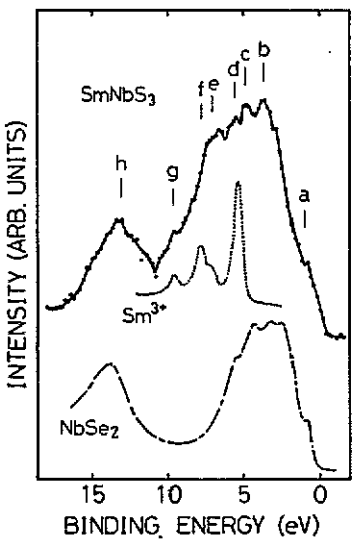

Figure 5. Comparison between the valence band XPS spectra of $SmNbS_3$ and $NbSe_2$ (Wertheim *et al* 1973) and Sm^{3+} in Sm metal (Baer and Busch 1974). The electronic structure of NbS_2 is quite similar to that of $NbSe_2$. The origin of the horizontal axis is the Fermi level.

Figure 7 shows the Sm $N_{4,5}$ ISEELS spectra of $SmNbS_3$ at $E_0 = 500$ eV and Sm metal at $E_0 = 315$ eV, where E_0 is the incident energy. It is found that their spectra are similar to each other because the near-edge structures are derived primarily from the atomic-like transitions of $4d^{10}4f^5$–$4d^94f^6$ within Sm^{3+}. The final state is known to be spread over a broad energy range by a strong exchange interaction between a 4d core hole and 4f electrons. Most of the oscillator strength is found in transitions to the high-energy $4d^94f^6$ states above the ionization threshold of the 4d electron, the peak being broadened by the autoionization process into the $4d^94f^5\epsilon$ f continua. Thus the ISEELS spectrum is composed of a broad peak modulated by various structures above the threshold and many fine structures below it. Strasser *et al* (1985) have found for Sm metal that the fine structures are reduced in intensity with increasing incident energy and the high-energy spectrum gives structures similar to the optical (x-ray) spectrum (Zimkina *et al* 1967, Haensel *et al* 1970). Since it is well known that, at high incident energies, an ISEELS spectrum in reflection geometry resembles

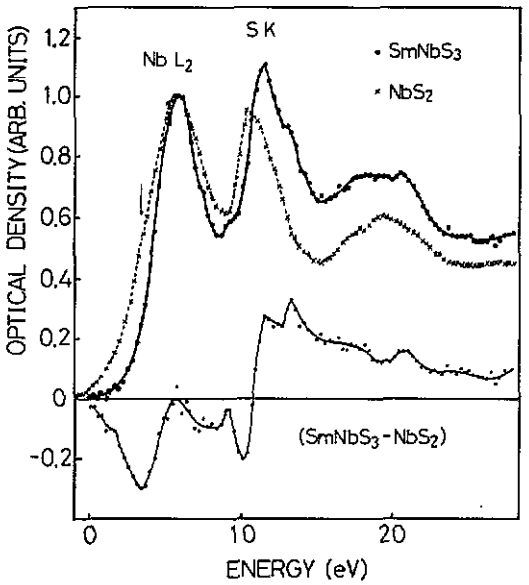

Figure 6. The Nb L_2 and S K x-ray absorption of $SmNbS_3$, compared with those of NbS_2. The lowest spectrum is the difference spectrum which has been obtained by subtracting the spectrum of NbS_2 from that of $SmNbS_3$.

the XAS spectrum which obeys dipole selection rules and, at low incident energies, optically forbidden transitions are also allowed owing to the breakdown of dipole selection rules by increased momentum transfer (Strasser *et al* 1985, Ohno 1987), this suggests that most of the transitions below the ionization threshold are optically forbidden. A slight difference between the spectra of $SmNbS_3$ and Sm metal may arise from the small contribution of the divalent component present near the metal surface (Wertheim and Campagna 1977, Wertheim and Crecelius 1978) or from the difference in the chemical environments which affects covalency and crystal-field effects.

Figure 8 shows the valence-electron-excited REELS spectra of $SmNbS_3$ and $SnNbS_3$ at $E_0 = 2000$ eV. A valence plasmon appears at 22.4 eV for $SmNbS_3$. This plasma energy and its incident-energy dependence almost coincide with those for NbS_2 and the value is largest of all the plasmon energies of the misfit-layer compounds measured up to now, although the free-electron value of 18.2 eV is smaller than those of $SnNbS_3$, $BiNbS_3$ and $SmTaS_3$. The incident-energy dependence of the plasma energy shown in figure 9 reveals a behaviour generally observed for a bulk plasmon unlike other misfit-layer compounds such as $SnNbS_3$ and $BiNbS_3$ in which the plasma energy decreases almost linearly with increasing incident energy. We shall discuss the excitation of plasmons of other misfit-layer compounds in detail in another paper (Ohno 1992). In contrast with the latter case the dependence for $SmNbS_3$ is easily explained in terms of the incident-energy dependence of momentum transfer in REELS and the dispersion relation of a free-electron plasmon. The fact that the valence plasma frequency and the incident-energy dependence are almost in agreement with those of NbS_2 may suggest that plasma oscillation in $SmNbS_3$ occurs three-dimensionally only within an NbS_2 layer. Such preferential plasma excitation is possible because, if the dispersion curve of a plasmon of SmS lies below the boundary of single-particle

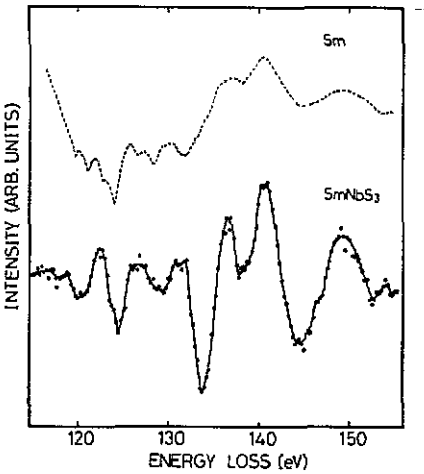

Figure 7. Sm $N_{4,5}$ ISEELS spectra of $SmNbS_3$ and Sm metal. Both spectra have been measured in the reflection mode. The spectrum of Sm metal is represented as an energy distribution curve as originally given by Strasser *et al* (1985) while the spectrum of $SmNbS_3$ is given in second-derivative form, using a lock-in amplifier.

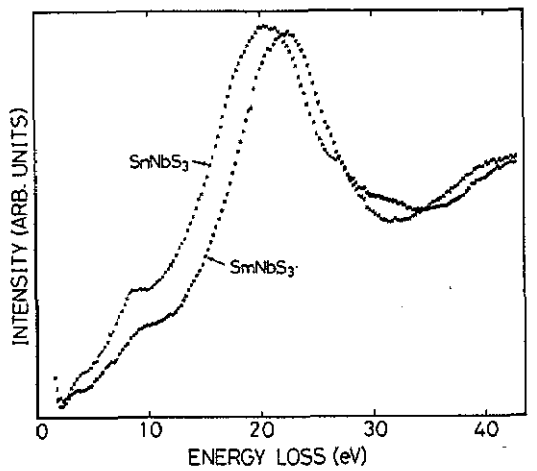

Figure 8. Valence-electron-excited REELS spectra of $SmNbS_3$ and $SnNbS_3$ measured at $E_0 = 2000$ eV in the pulse-counting mode.

excitation, plasma oscillation within an SmS layer decays rapidly.

Figure 10 shows the second-derivative REELS spectra at various low incident energies. As can be seen from figure 10, interband transitions are dominant in the low-incident-energy spectrum because plasmons decay into single-particle excitation with decreasing incident energy. The energies of the main features are summarized in table 3 together with those of $SnNbS_3$. It is surprising that the spectra are quite similar to those of $SnNbS_3$ in spite of the large difference between the electronic structures of the SmS and SnS layers. This may be because the Sm 4f levels are well localized and the S 3p bands of the SmS layers overlap the valence bands of NbS_2 at about 4–5 eV below the Fermi level. A recent self-consistent APW calculation

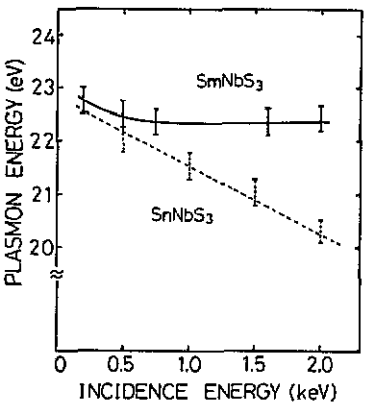

Figure 9. Plasmon energies of $SmNbS_3$ and $SnNbS_3$ as functions of incident energy.

for SmS indicates that unoccupied 4f levels are shifted by 5.5 eV from occupied 4f levels owing to strong Coulomb correlation interaction and are hybridized with other extended orbitals such as S 3d and Sm 5d orbitals (Aguilar and Quintana 1986). However, the hybridization is weaker than that in other f systems. Since pure 4f–4f transitions are optically forbidden, the low-energy structures are derived predominantly from S 3p–Sm 5d transitions. The onset energy has been estimated by Batlogg *et al* (1976) to be about 3 eV. Their optical data also give the energy separations between crystal-field-split 5d t_{2g} and e_g peaks and between the S 3p and Sm 5d t_{2g} peaks to be 2.36 eV and 4.8 eV, respectively. Then S 3p–Sm 5d interband transitions may contribute to loss structures at 5.8 and 8.4 eV. The partial resonance plasmon of Nb d electrons within an NbS_2 layer results in a large peak at around 8 eV (Bell and Liang 1976, Tosatti and Girlanda 1986). The assignments of the main features have been carried out using the previous discussion for $SnNbS_3$ (Ohno 1991a). They are summarized in table 3. The plasma resonance of free conduction electrons, which has been observed at 2.45 eV in the pressure-induced metallic phase of SmS (Batlogg *et al* 1976), is not observed. This implies that the electronic structure near the Fermi level is different in an SmS layer in $SmNbS_3$ from that in metallic SmS.

4. Conclusions

The Sm 3d and 4d XPS studies have confirmed the previous suggestion from the lattice parameter measurement that Sm in $SmNbS_3$ is triply ionized, as has been found in pressure-induced metallic SmS. It is, however, considered that, in metallic SmS, the Sm^{3+} ions are induced by a reduction in the Sm–S and Sm–Sm distances owing to the applied external high pressure while in $SmNbS_3$ they are induced by charge transfer from SmS to NbS_2 layers, which results in short average Sm–S and Sm–Sm distances because of the smaller ionic radius of Sm^{3+}. From the viewpoint of electronic structure, a reduction in the lattice parameter of SmS leads to the intersection of occupied 4f levels with 5d conduction bands, resulting in one free 5d conduction electron per cation and bringing about the semiconductor–metal transition, whereas in $SmNbS_3$ the charge transfer of Sm 4f electrons into the incompletely filled Nb d_{z^2} band causes a change in the valence state of Sm from divalent to trivalent and a shift in the Fermi level within an NbS_2 layer upwards, but does not induce intersection of

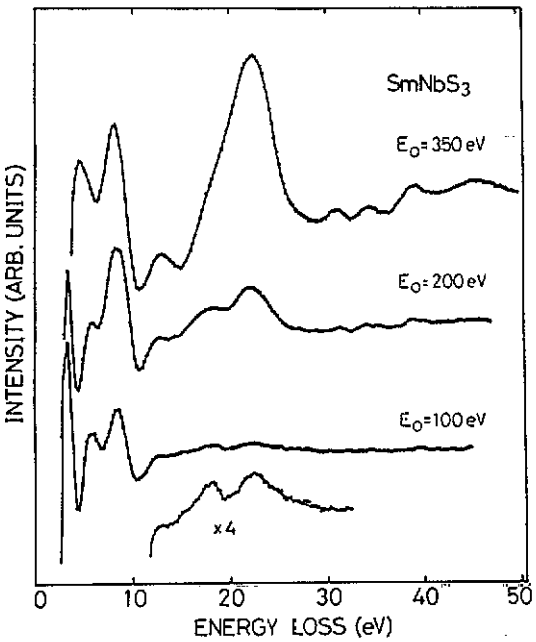

Figure 10. Second-derivative REELS spectra of $SmNbS_3$ at various low incident energies, which have been measured in the voltage modulation mode at an applied voltage of 1 V peak to peak. The energy resolution increases with decreasing incident energy.

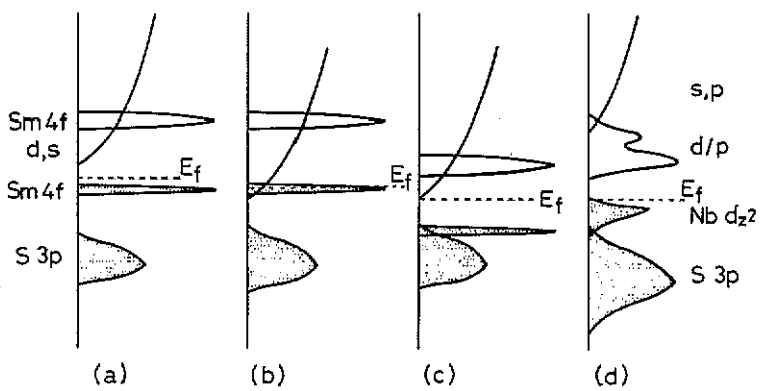

Figure 11. Schematic energy band structures of (*a*) semiconducting SmS, (*b*) pressure-induced metallic SmS, (*c*) an SmS layer in $SmNbS_3$ and (*d*) an NbS_2 layer in $SmNbS_3$. In the semiconducting phase the Fermi level is located just above the occupied 4f band, but below the 5d conduction bands, whereas in the pressure-induced metallic phase it is located within the occupied 4f band because the 5d bands are broadened by the reduced Sm–S and Sm–Sm distances and overlap the occupied 4f band, leading to charge transfer of a fractional part of a 4f electron into the 5d bands. In an SmS layer the 4f occupied band shifts downwards in energy because of the stronger Coulomb potential of Sm^{3+}. Therefore, if the 5d conduction bands do not overlap the Nb d_{z^2} band, the SmS layers remain semiconducting.

Table 3. Energies of the main features of the REELS spectra of $SmNbS_3$ and $SnNbS_3$.

Energy (eV)		
$SmNbS_3$	$SnNbS_3$ [a]	Assignment
3.3	3.5	Interband transitions in an NbS_2 layer
5.8	5.7	Interband transitions in SmS (SnS) and NbS_2 layers
8.4	8.0	Plasmon of d electrons in an NbS_2 layer
12.5 15.0	12.9	Interband transitions to conduction bands of higher energy than the Nb d bands
18.1	17.5	Bulk plasmon in an SmS (SnS) layer and interband transitions from S 3s bands
22.7	22.5	Bulk plasmon in an NbS_2 layer
31.3 34.5 39.0	32.2 35.0 39.2	Nb $N_{2,3}$ transitions

[a] Ohno (1991a).

the 4f levels with the 5d conduction bands within an SmS layer because after charge transfer the $4f^5$ (^6H) levels shift downwards in energy with respect to the $4f^6$ (^7F) levels or the 5d conduction bands by about 4 eV because of a stronger Coulomb potential. Thus we may expect that, if the 5d bands do not overlap the Nb d_{z^2} band, the SmS layers remain semiconducting. They are shown in figure 11 schematically. Since many XPS, XAS and REELS results obtained to date support the occurrence of charge transfer from the MS to TS_2 layers, it is believed that charge transfer is a common feature for the misfit-layer compounds. Therefore we may regard these materials as donor-type intercalation derivatives of a layered TS_2 compound. The XPS spectra have shown that valence mixing is very small, if it occurs. It has been estimated that the number of Sm^{2+} ions is less than a few per cent of the number of Sm^{3+} ions. The fact that the plasma frequency of the valence plasmon is the same as that of NbS_2 suggests that plasma oscillation occurs only within an NbS_2 layer. Such preferential plasma excitation is possible if the dispersion curve of the valence plasmon of SmS lies below the boundary of single-particle excitation.

References

Aguilar F L and Quintana J C 1986 *J. Phys. C: Solid State Phys.* **19** 2485
Baer Y and Busch G 1974 *J. Electron Spectrosc.* **5** 611
Batlogg B, Kaldis E, Schlegel A and Wachter P 1976 *Phys. Rev.* B **14** 5503
Bearden J A 1967 *Rev. Mod. Phys.* **39** 78
Bell M G and Liang W Y 1976 *Adv. Phys.* **25** 53
Campagna M, Bucher E, Wertheim G K and Longinotti L D 1974 *Phys. Rev. Lett.* **33** 165
Chazalviel J N, Campagna M, Wertheim G K and Schmidt P H 1976 *Phys. Rev.* B **14** 4586
Dufour G, Karnatak R C, Mariot J M and Bonnelle C 1976 *Chem. Phys. Lett.* **42** 433
Haensel R, Rabe P and Sonntag B 1970 *Solid State Commun.* **8** 1845
Jayaraman A, Bucher E, Dernier P D and Longinotti L D 1973 *Phys. Rev. Lett.* **31** 700

Jayaraman A, Narayanamurti V, Bucher E and Maines R G 1970 *Phys. Rev. Lett.* **25** 1430
Jo T and Kotani A 1988 *Phys. Rev.* B **38** 830
Kotani A 1987 *J. Phys. C: Solid State Phys.* **9** 869
Kowalczyk S P, Edelstein N, McFeely F R, Ley L and Shirley D A 1974 *Chem. Phys. Lett.* **29** 491
Krill G, Senateur J P and Amamou A 1980 *J. Phys. F: Met. Phys.* **10** 1889
Lang J K, Baer Y and Cox P A 1981 *J. Phys. F: Met. Phys.* **11** 121
Meerschaut A, Auriel C, Lafond A, Deudon C, Gressier P and Rouxel J 1991 *Eur. J. Solid State Inorg. Chem.* **28** 581
Oh S J and Allen J W 1984 *Phys. Rev.* B **29** 589
Ohno Y 1987 *Phys. Rev.* B **36** 7500
—— 1991a *Phys. Rev.* B **44** 1281
—— 1991b *Solid State Commun.* **79** 1081
—— 1992 *Phys. Rev.* at press
Ohno Y, Hirama K, Nakai S, Sugiura C and Okada S 1983 *Phys. Rev.* B **27** 3811
Ohno Y, Kaneda K and Hirama K 1984 *Phys. Rev.* B **30** 4648
Strasser G, Rosina G, Matthew J A D and Netzer F P 1985 *J. Phys. F: Met. Phys.* **15** 739
Tosatti E and Girlanda R 1986 *Electronic Structure and Electronic Transitions in Layered Materials* ed V Grasso (Boston, MA: Reidel)
Wagner C D, Riggs W M, Davis L E, Moulder J F and Muilenberg G E 1979 *Handbook of X-ray Photoelectron Spectroscopy* (Eden Prairie, MN: Perkin-Elmer)
Wertheim G K and Campagna M 1977 *Chem. Phys. Lett.* **47** 182
Wertheim G K and Crecelius G 1978 *Phys. Rev. Lett.* **40** 813
Wertheim G K, DiSalvo F J and Buchanan D N E 1973 *Solid State Commun.* **13** 1225
Wiegers G A, Meetsma A, Haange R J, Van Smaalen S, de Boer J L, Meerschaut A, Rabu P and Rouxel J 1990 *Acta Crystallogr.* B **46** 324
Wiegers G A, Meetsma A, Van Smaalen S, Haange R J, Wulff J, Zeinstra T, de Boer J L, Kuypers S, Van Tendeloo G, Van Landuyt J, Amelinckx S, Meerschaut A, Rabu P and Rouxel J 1989 *Solid State Commun.* **70** 409
Zimkina T M, Fomichev V A, Gribovskii S A and Zhukova I I 1967 *Sov. Phys.–Solid State* **9** 1128